THE JOURNAL OF PHYSICAL CHEMISTRY C

Article

pubs.acs.org/JPCC

Predicting Energy Conversion Efficiency of Dye Solar Cells from First Principles

Wei Ma, Yang Jiao, and Sheng Meng*

Beijing National Laboratory for Condensed Matter Physics and Institute of Physics, Chinese Academy of Sciences, Beijing, 100190, People's Republic of China

Collaborative Innovation Center of Quantum Matter, Beijing, China

Supporting Information

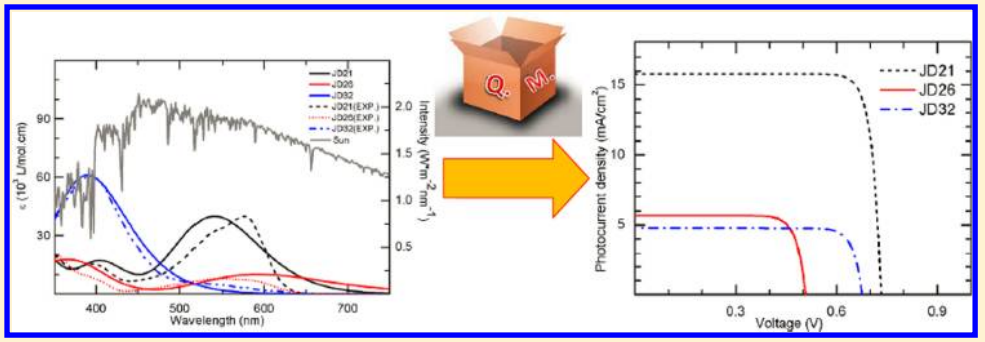

ABSTRACT: In this work we target on accurately predicting energy conversion efficiency of dye-sensitized solar cells (DSC) using parameter-free first principles simulations. We present a set of algorithms, mostly based on solo first principles calculations within the framework of density functional theory, to accurately calculate key properties in energy conversion including sunlight absorption, electron injection, electron−hole recombination, open circuit voltages, and so on. We choose two series of donor-π-acceptor dyes with detailed experimental photovoltaic data as prototype examples to show how these algorithms work. Key parameters experimentally measured for DSC devices can be nicely reproduced by first-principles with as less empirical inputs as possible. For instance, short circuit current of model dyes can be well reproduced by precisely calculating their absorption spectra and charge separation/recombination rates. Open circuit voltages are evaluated through interface band offsets, namely, the difference between the Fermi level of electrons in TiO_2 and the redox potential of the electrolyte, after modification with empirical formulas. In these procedures the critical photoelectron injection and recombination dynamics are calculated by real-time excited state electronic dynamics simulations. Estimated solar cell efficiency reproduces corresponding experimental values, with errors usually below 1−2%. Device characteristics such as light harvesting efficiency, incident photon-to-electron conversion efficiency, and the current−voltage characteristics can also be well reproduced and compared with experiment. Thus, we develop a systematic ab initio approach to predict solar cell efficiency and photovoltaic performance of DSC, which enables large-scale efficient dye screening and optimization through high-throughput first principles calculations with only a few parameters taken from experimental settings for electrode and electrolyte toward a renewable energy based society.

1. INTRODUCTION

Dye-sensitized solar cells (DSC) based on highly porous nanocrystalline titanium dioxide films have drawn considerable technological interest for their potential to decrease manufacturing costs and demonstrated high power energy conversion efficiency since the seminal work of Grätzel et al. in 1991.[1] The highest solar-to-electrical power conversion efficiency (PCE) for molecular DSC is 12.3% under AM1.5G full sun irradiation, obtained by cosensitization of zinc porphyrin dye with another donor-π-acceptor (D-π-A) dye in 2011.[2] Wang et al. have recently achieved comparable efficiency of 12.8% at *half* irradiance of the AM1.5G sunlight using metal-free organic dyes, which possess larger molar absorption coefficient, benign environment impact, and low cost compared with dyes containing heavy metals.[3] Moreover, the newly designed solid-state perovskite sensitized solar cells have been reported to achieve a PCE of approximately 15% under standard AM1.5G irradiation.[4] However, these efficiencies are still low compared to that needed for large-scale implementation.

DSC operates by harvesting incident photons and converting solar energy into electricity. Upon photoexcitation, the absorbed photon excites one electron from the highest occupied molecular orbital (HOMO) to the lowest unoccupied molecular orbital (LUMO) of the sensitizer, then the electron

Special Issue: Michael Grätzel Festschrift

Received: November 7, 2013
Revised: January 8, 2014
Published: January 9, 2014

 © 2014 American Chemical Society dx.doi.org/10.1021/jp410982e | J. Phys. Chem. C 2014, 118, 16447−16457

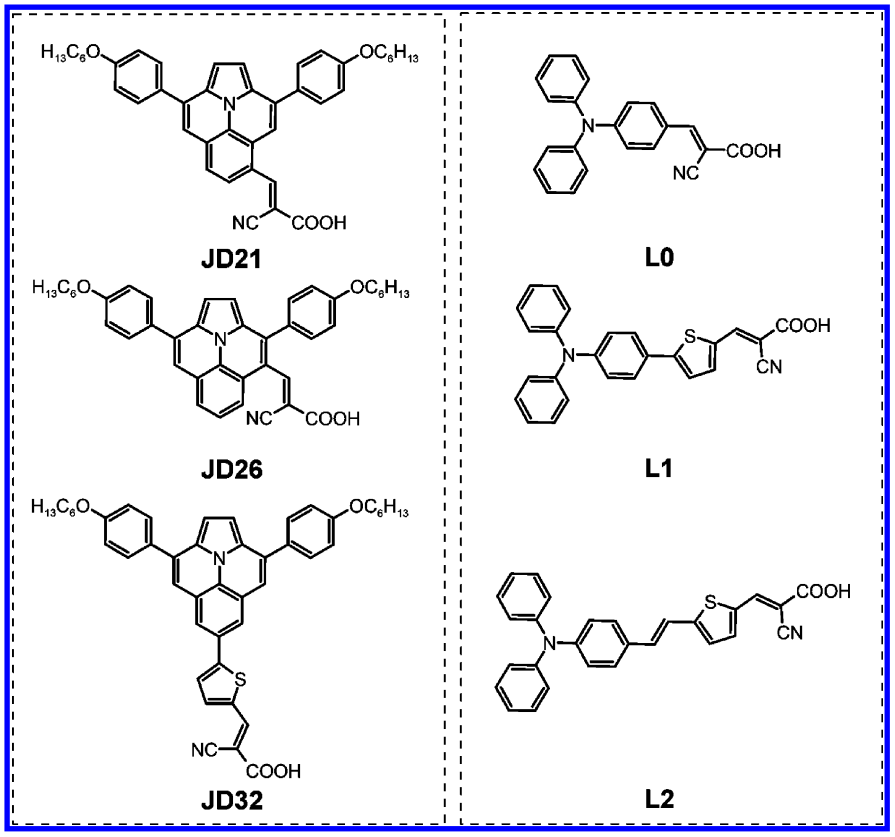

Figure 1. Chemical structures of JD-dyes and L-dyes.

injects from the LUMO of the chromophore to the semiconductor (TiO_2) conduction band (CB); meanwhile, the oxidized dye is regenerated to the ground-state by a redox shuttle. At last, the separated electron and hole diffuse toward electrical contacts where they are collected. During this whole electronic dynamic process, the electron injection efficiency to the TiO_2 CB and the electron collection efficiency at the transparent conductive oxide electrode directly determine the short circuit current density (J_{SC}) of DSC. The potential difference between the Fermi level of electrons in the semiconductor substrate and the redox potential of the electrolyte gives the open circuit photovoltage (V_{OC}). These two parameters are important factors determining the DSC energy conversion efficiency.

$$\eta = \mathrm{FF}\frac{J_{SC}V_{OC}}{P_{inc}} \quad (1)$$

The FF is the fill factor at which DSC operates with the maximum power, which is mainly related to the total series resistance of the DSC. P_{inc} is the input power of incident solar light.

During the past decades, great efforts have been made to improve the energy conversion efficiency of DSC, which can be mainly classified into three kinds: (i) increasing the light harvesting of the sensitizer; (ii) enhancing efficient electron injection; (iii) retarding the electron−hole recombination. For example, Chiba et al. achieved an efficiency of 11.1% by enhancing the light harvesting efficiency using the so-called black dye.[5] Hardin et al. broadened further the absorption spectra of ruthenium metal complex dyes by harvesting high-energy photons using Förster energy transfer.[6] Delcamp et al. designed a new series of donor-π-acceptor structure dyes to provide efficient electron injection because of a pronounced push−pull effect.[7] Haid et al. retarded the electron−hole recombination by about five times through a tiny structural modification of the sensitizer.[8] However, the exponential increase in research efforts has not been matched by a dramatic increase in efficiency. A major part of human and material resources have been invested in synthesis and characterization of newly designed dyes, with few of which contribute to improvements in DSC device performance. Recently Labat et al. have qualitatively predicted the properties of isolated components of DSC assemblies using density functional theory (DFT) based modeling,[9] however, high-precision prediction of solar cell efficiency based on direct first principles dynamics and the known chemical composition of sensitizer has been a daunting task. If one could estimate the DSC efficiency with high accuracy, great efforts would be saved for better focused and effective research.

The PCE of the DSC is closely related to its light harvesting efficiency, the electron injection efficiency, and collection efficiency. Therefore, if the absorption properties of the sensitizer, the electron injection and electron−hole recombination lifetime of the DSC can be precisely calculated, the PCE could be nicely predicted. Time-dependent density functional theory (TDDFT) with large atomic basis sets and proper selection of exchange-correlation functionals is demonstrated to perform well in describing the polarizability and optical excitation spectrum of most organic and inorganic dyes.[10,11] Thus, the UV−vis spectra of the investigated chromophores can be nicely obtained. Therefore, the remaining question is to accurately calculate the electron injection and charge recombination dynamics in DSC.

dx.doi.org/10.1021/jp410982e | J. Phys. Chem. C 2014, 118, 16447−16457

Usually empirical theoretical approaches have been routinely employed to deal with critical interface electron dynamics including photoelectron injection and recombination at the dye/TiO_2 interface. These approaches are mainly based on optimized structural features and ground-state molecular dynamics simulations, and/or with empirical kinetic parameters, such as assuming an exponential decay of electron injection rate as a function of dye length[12,13] and constant electron coupling strength.[14] For instance, Persson et al. have studied the influence of anchor-cum-spacer groups on electron transfer time by approximating the effective electronic coupling strength with the calculated bandwidth for heterogeneous electron transfer interactions based on ground-state DFT calculations.[15] Abuabara et al. successfully investigated the influence of temperature changes on electron injection at dye/TiO_2 interface using ground-state molecular dynamics and studied the electron transfer process using an extended Hükel Hamiltonian.[16] Prezhdo et al. reproduced injection dynamics of model chromophores with atomistic details using ground state molecular dynamic simulation and time domain nonadiabatic trajectory surface hopping based on ground-state trajectories.[17−19] Li et al. studied electron transfer from perylene derivatives into the anatase TiO_2 (101) surface using DFT and a Fock matrix partitioning method.[20] Jones et al. could rapidly predict the injection rate in DSC by partitioning the system into molecular and semiconductor subsystems and computing the retarded Green's function.[21] However, there are some problems associated with these empirical models: (i) The excited state potential energy surfaces (PES), which are different from ground state PES, are missing in these simulations, thus the electronic properties in excited states cannot be addressed adequately. (ii) The electronic couplings at the interface, which is subject to molecular details of the dyes and their dynamic binding configurations on TiO_2, cannot be described precisely; thus, the time scales obtained therein are questionable. In addition, only a few of these studies have been devoted to investigating charge recombination processes,[22,23] where they suffer from the same problems mentioned above. Directly monitoring electron transfer dynamics, especially for recombination, across the chromophore−semiconductor interface is strongly needed for a better understanding of interface electronic dynamics. In previous work,[24,25] we have demonstrated that our approach using real-time time-dependent density functional theory, which evolves quantum mechanically the wave functions of excited electron−hole pair at the dye/TiO_2 interface based on excited state Hamiltonian, is especially adequate to treat the interface electronic dynamics and yield consistency with experiment. Therefore, this method is promising to give best estimations of the DSC power conversion efficiency.

Here we present a systematic ab initio approach based on DFT and time-dependent DFT to accurately predict the PCE of DSC. To demonstrate how this algorithm works, we adopt ullazine dyes (JD-dyes) with an electron-rich heterocycle and L-dyes with the triphenylamine donor and the cyanoacetic acid acceptor as sample dyes (Figure 1). By calculating the absorbance of the sensitizers and the injection and recombination lifetimes at the dye/TiO_2 interface using real-time excited state electronic dynamics simulations based on TDDFT, J_{SC}, and V_{OC} are nicely reproduced with few empirical inputs. The light harvesting efficiency (LHE), incident photon-to-electron conversion efficiency (IPCE) and the current−voltage (I−V) characteristics are also calculated and demonstrated to be comparable with experiment. Herein, V_{OC} is evaluated through two models, both based on the potential difference between the electrolyte redox potential and the quasi-Fermi level of electrons in the semiconductor TiO_2. By taking recombination rate into consideration, the second model[26] is illustrated to yield more reasonable estimates than model-I,[27] which considers only effects of dye adsorption on the interface electronic structure. In this way, the PCE of DSC is obtained with errors usually below 1−2% comparing with corresponding experimental values. Here a set of predictive algorithms for nanodevice operation rate assessment (PANDORA) are presented. We thus develop a systematic ab initio approach to predict solar cell efficiency and photovoltaic performance of DSC, enabling large-scale efficient dye screening and optimization through high-throughput first principles calculations for renewable energy.

2. METHODOLOGY

2.1. Computational Methods and Models. First-principles density functional theory[28] calculations were carried out to study the molecular geometries and electronic structures of the sensitizers adsorbed onto TiO_2 surfaces. The ground-state molecular geometries were optimized with SIESTA,[29] using the pseudopotentials of the Troullier-Martins type[30] to model the atomic cores, the Perdew-Burke-Ernzerhof (PBE) exchange-correlation functional,[31] and a local basis set of double-ζ polarized (DZP) orbitals (19 numerical atomic orbitals for Ti including semicore 3 s and 3 p states;[32] 13 orbitals for C, N, O, and S; 5 orbitals for H). An auxiliary real space grid equivalent to a plane wave cutoff of 150 Ry and Γ point k-sampling was used. Geometries were optimized until forces on nonfixed atoms are below 0.005 eV/Å, which were considered fully relaxed. The stoichiometric anatase (101) surface, the dominant facet in DSC devices,[33] was modeled with a periodically repeated slab. A large simulation cell, 10.24 × 15.14 × 30.00 $Å^3$, containing a 96-atom (4 × 1) surface with six atomic layers of TiO_2 and organic chromophores was adopted, corresponding to a surface coverage of one dye per 155 $Å^2$ or 1.07 μmol·cm^{-2}. The slab was separated from its periodic images along the surface normal by a vacuum region of ∼10 Å. To justify the basis set we used for dye/TiO_2 systems, we also made calculations with diffusive basis set of S atom (15 numerical atomic orbitals including two diffusive 4 s states). The inclusion of diffusive basis sets to S atoms leads to negligible differences in the bond length (∼0.002 Å) and bond angles (∼0.1°) of the dye molecules, as well as a small energy difference (≤0.01 eV) in the band positions. Optical absorption spectra were calculated based on linear response TDDFT using the B3LYP and CAM-B3LYP functional and 6-31G(d) basis set, as implemented in Gaussian 09 program. The Polarizable Continuum Model[34] was used to account for the solvation effect (in CH_2Cl_2).

2.2. Electronic Dynamics Simulation. In our simulations of electron injection and electron−hole recombination processes, the evolution of both electrons and ions in real time is monitored after photo excitation.[35] The time-dependent Kohn−Sham equations of electrons and the Newtonian motion of ions are solved simultaneously, with ionic forces along the classical trajectory evaluated through the Ehrenfest theorem. The electron density is updated self-consistently during the real time propagation of Kohn−Sham wave functions with a time step of 0.02419 fs. The initial velocity of ions is assigned according to the equilibrium Boltzmann-Maxwell distribution at

dx.doi.org/10.1021/jp410982e | J. Phys. Chem. C 2014, 118, 16447−16457

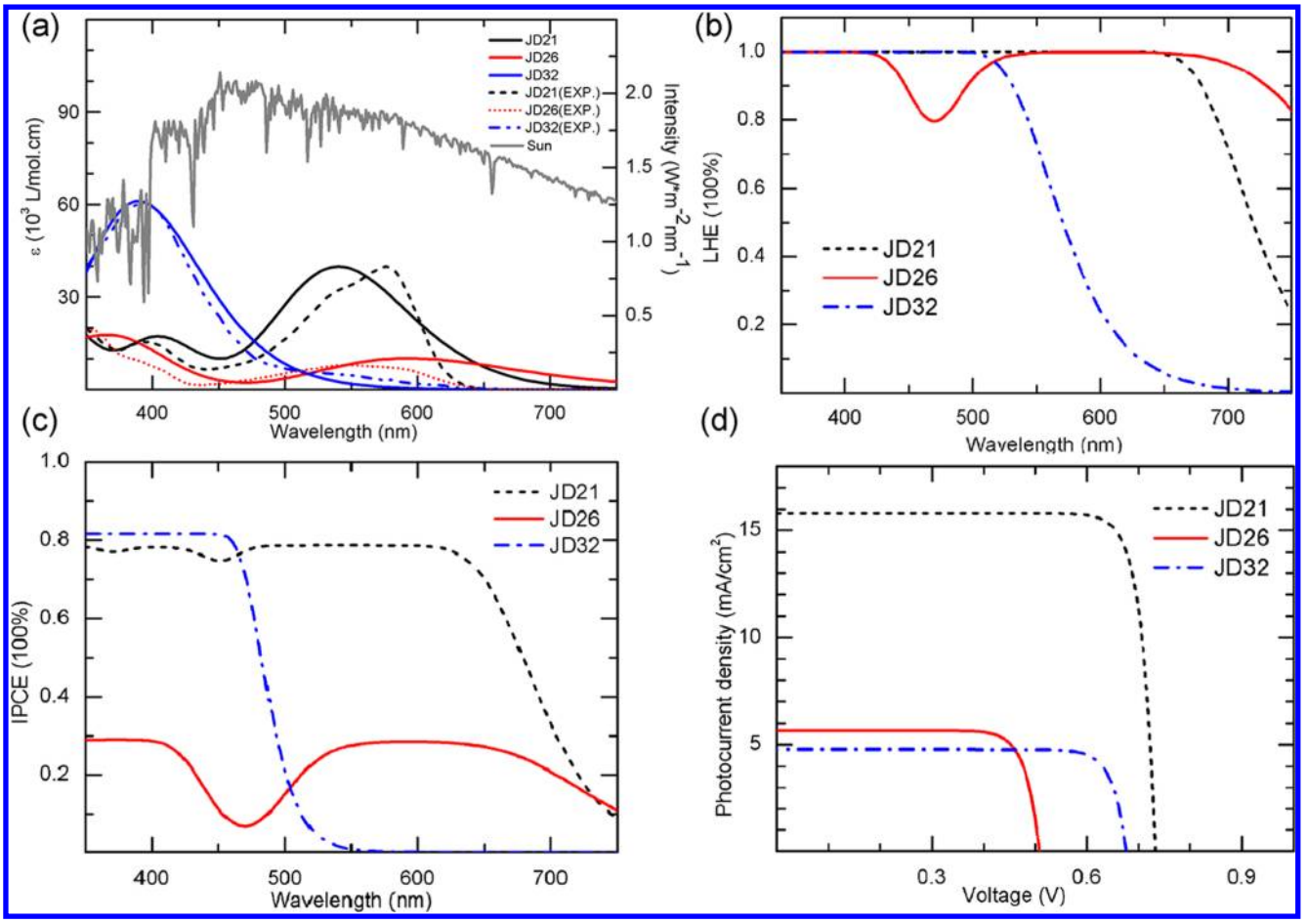

Figure 2. (a) Calculated and experimental absorption spectra of JD-dyes using B3LYP/6-31G(d) with PCM model of CH_2Cl_2 solution. The gray line is the solar spectrum. (b) Calculated light harvesting efficiency of JD-dyes. (c) Calculated spectra of monochromatic incident phonon to current conversion efficiency of JD-dyes. (d) Calculated $I-V$ curve of JD-dyes.

a given temperature of 350 K. Within this scheme, the total energy is well conserved to within 10^{-4} eV/fs, which is proved to be accurate enough to produce negligible differences in energy levels evolution and electron-ion dynamics. Although the standard functionals do not treat charge-transfer excitation well, long-range corrected functional should be more accurate for excitation energies. In our dynamical simulation, the exact excitation energy is not the focus but the energy alignment and the time scales. We have shown in the previous work that the energy level alignment is correctly reproduced by DFT with PBE functional.[36]

3. RESULTS AND DISCUSSION

3.1. Electronic Structure and Photoabsorption of Organic Dyes. Metal-free donor-π bridge-acceptor dyes are particularly promising for their large molar extinction coefficients, efficient photoelectron injection due to the pronounced push−pull effect, and comparable PCEs but more cost-effective properties comparing with metal-complex dyes. Figure 1 shows the chemical structures of two prototype kinds of D-π-A dyes: the ullazine-based JD-dyes[7] and the triphenylamine-based L-dyes.[37] Ullazine is a 16 π-electron nitrogen-containing heterocyclic unit, which possesses a planar π-system to promote strong intramolecule charge transfer with both efficient electron donating and accepting properties. JD21 and JD26 are isomers with the cyanoacetic acid group in the ortho-position and meta-position of the ullazine core, respectively. JD32 has an additional thiophene group and a substitution site of para-position, comparing to JD21 and JD26 dyes. The insertion of the thiophene group into JD32 dye is to drastically shift its optical absorption to visible light region and to directly compare calculated properties with available experimental data.[7] L-dyes consist of a triphenylamine donor and a cyanoacetic acid acceptor. By introducing thiophene between the triphenylamine donor and cyanoactic acid acceptor to extend the number of π-conjugation groups, the molecular HOMO and LUMO energy levels can be tuned, resulting in a red-shifting and broadening in optical absorption peaks.

The photoabsorption of these dyes was calculated using TDDFT with B3LYP and CAM-B3LYP functional and 6-31G(d) basis sets (see Figure 2a and 3a). The Polarizable Continuum Model (PCM) was used to account for the solvation effect in CH_2Cl_2 for JD-dyes. Calculated spectra for JD dyes are shown in Figure 2a. The position of first absorption peak is correlated with the ground-state HOMO−LUMO gap, but with the electron−hole interactions and the screening effects included. Our simulation results of absorption maximum are 539 nm for JD21, 593 nm for JD26, and 394 nm for JD32, agree well with the experiment values (582 nm for JD21, 548 nm for JD26, and 393 nm for JD32, respectively).[7] In addition, the calculated molar extinction coefficients are also consistent with experimental values. In Figure 3a, the first optical absorption band of L0, L1, and L2 are located at 374, 426, and 463 nm, which agrees well with experimental values for L

dx.doi.org/10.1021/jp410982e | J. Phys. Chem. C 2014, 118, 16447−16457

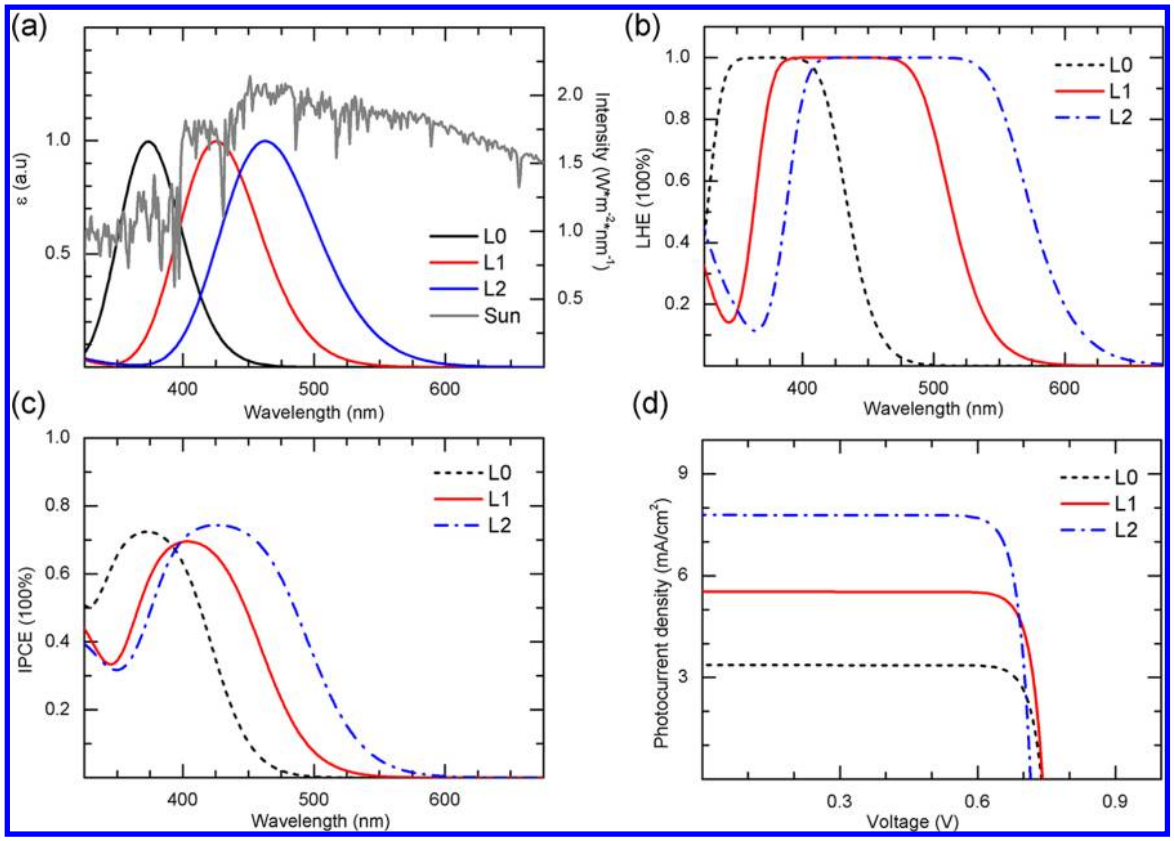

Figure 3. (a) Normalized UV−vis absorption spectra of L-dyes using CAM-B3LYP/6-31G(d). The gray line is the solar spectrum. (b) Calculated light harvesting efficiency of L-dyes. (c) Calculated spectra of monochromatic incident phonon to current conversion efficiency of L-dyes. (d) Calculated *I*−*V* curve of L-dyes.

dyes (373 nm for L0, 404 nm for L1, and 427 nm for L2).[37] The absorption maximum is significantly red-shifted as the conjugation length increases, indicating a larger sunlight harvesting efficiency of the longer dyes (Figure 3b).

3.2. Dye Adsorption and Interface Binding. The interface structure upon dye adsorption is of crucial importance to determine the interface energy alignment, thus affecting the photovoltaic performance of DSC devices. Here, we found the sensitizers bind to the TiO_2 substrate via tridentate bridging mode, with two interface O−Ti and N−Ti bonds and an additional hydrogen bond connected to the O atom of the TiO_2 substrate (Figure 4a−f). This tridentate anchoring mode resulted in a most stable adsorption configuration with adsorption energies 1.16, 1.18, and 1.20 eV for dyes JD21, JD26, and JD32, respectively. While for L-dyes, the same binding structures lead to an adsorption energy of 1.37 eV for L0, 1.48 eV for L1, and 1.55 eV for L2. This result is perfectly consistent with our previous calculations.[24,36]

The alignment of electronic levels of the dye/TiO_2 system has also been calculated. Figures 4g−i show the projected density of states (PDOS) of dyes JD21, JD26, and JD32, where the energy is measured referring to the vacuum energy level. The calculated LUMO of the sensitizer lies above the conduction band minimum (CBM) of the semiconductor TiO_2 substrate (about −4.0 eV vs vacuum), which ensures an efficient electron transfer from the excited dye to the TiO_2 conduction band. Meanwhile, the HOMO lies in the gap between the conduction band and valence band (VB), more negative than the iodide/triiodide redox potential, indicating energetically favorable ground-state dye regeneration. The

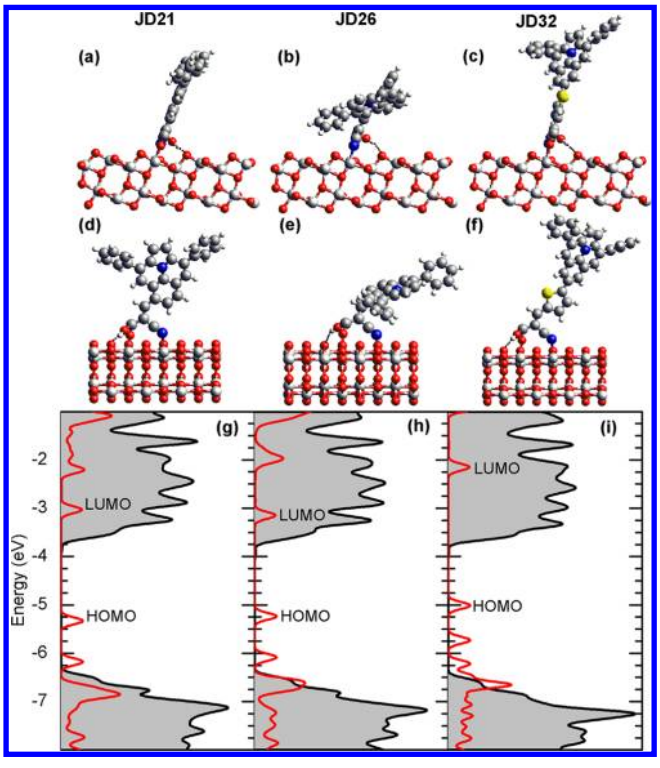

Figure 4. (a−c) Front view and (d−f) side view of JD-dyes adsorption configurations. (g−i) Calculated projected density of states for JD21, JD26, and JD32 dyes. Red curves are for the dyes, and shaded areas under black lines are for TiO_2 substrate.

dx.doi.org/10.1021/jp410982e | J. Phys. Chem. C 2014, 118, 16447−16457

calculated energy levels of HOMO, LUMO, CBM, and valence band maximum (VBM) are listed in Table 1. The PDOS of the

Table 1. Energy Levels and Driving Forces of the JD-Dyes and L-Dyes Calculated from First Principles

dye	VBM (eV)	HOMO (eV)	CBM (eV)	LUMO (eV)	E_g (eV)	ΔG^0_{inj} [a] (eV)	ΔG^0_{rec} [b] (eV)
JD21	−6.49	−5.33	−3.59	−3.04	2.29	0.55	1.74
JD26	−6.53	−5.24	−3.63	−3.15	2.09	0.48	1.61
JD32	−6.46	−5.02	−3.63	−2.17	2.85	1.46	1.39
L0	−6.69	−5.28	−4.08	−3.57	1.71	0.51	1.20
L1	−6.69	−5.11	−4.06	−3.71	1.40	0.35	1.05
L2	−6.69	−5.02	−4.07	−3.77	1.25	0.30	0.95

[a]Driving force for electron injection $\Delta G^0_{inj} = E_{LUMO} - E_{CBM}$. [b]Driving force for charge recombination $\Delta G^0_{rec} = E_{CBM} - E_{HOMO}$.

L-dyes are also calculated (shown in Supporting Information, Figure S1), which are similar to the alignment of JD-dyes, revealing efficient dye regeneration and fast electron injection properties.

3.3. Electron Dynamics at the Interface from First Principles. In order to functionalize an efficient DSC, ultrafast photoelectron injection and sluggish recombination are of necessity. We monitor the charge injection and recombination processes between the sensitizer and the semiconductor TiO_2 substrate using TDDFT. Our TDDFT approach has advantages in several aspects: (i) Very efficient atomic orbital basis sets are adopted, which are small in size and fast in performance. (ii) Either periodic system or a finite-sized supercell with large vacuum space can be treated without heavy calculation cost. (iii) Real time excited state trajectories with many-electron density self-consistently propagating at every electronic and ionic steps and forces calculated from mean-field theory are achieved. The validity of the present method is verified by comparing the calculated injection times to available experimental ones. Our previous calculations show that the excited electrons in the cyanin dye injected into TiO_2 substrate with a time scale of ~72 fs,[38] in agreement with the experimental measurements of ≤100 fs.[39] A femtosecond laser study of the alizarin sensitized TiO_2 indicated an electron injection time of 6 fs.[40] Our simulation found a consistent ultrafast injection time of 12 fs correspondingly. Comparison to some experimental injection times for representative dyes is listed in Table 1 of ref 41. In this circumstance, we can successfully deal with the electron-ion dynamics at the dye/TiO_2 interface using the full TDDFT treatment.

Figure 5 shows the fractions of photoelectrons injected into the substrate as a function of time after excitation of the JD-dyes. One electron is promoted from the HOMO to the LUMO of the organic dyes at the beginning of the simulation, representing the first excited state that a pair of electron and hole is generated upon photon absorption. Electronic state diagonalization is performed at this first step after the occupation switch. Then the coupled electron-ion system evolves in real time. The initial ionic temperature is set to 350 K. We found that the electrons are slightly distributed on the TiO_2 at $t = 0$, due to the electronic coupling between the dye and the TiO_2 substrate. Then the amount of excited electrons on the substrate increases slowly at the first 200 fs but is rapidly boosted exponentially after 200 fs. At last, excited electrons are completely injected into the CB of the TiO_2 substrate within a time scale of 290 fs for JD21, 240 fs for JD26, and 400 fs for

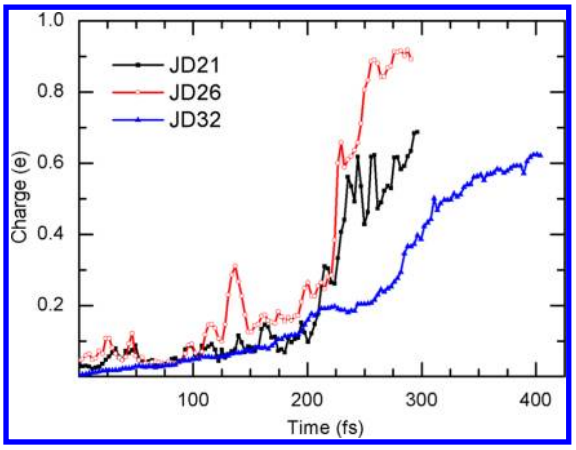

Figure 5. Fraction of electrons injected to the TiO_2 semiconductor substrate as a function of time after photoexcitation at the organic dye/TiO_2 interface.

JD32, while holes are kept stable and confined within the dye molecules. Here the lifetime of the injection process is estimated by the time when 63.2% electrons are transferred from the sensitizer into the TiO_2 electrode.

Figure 6 shows the electron recombination dynamics of JD-dyes. Unlike the electron injection process, the initial states of

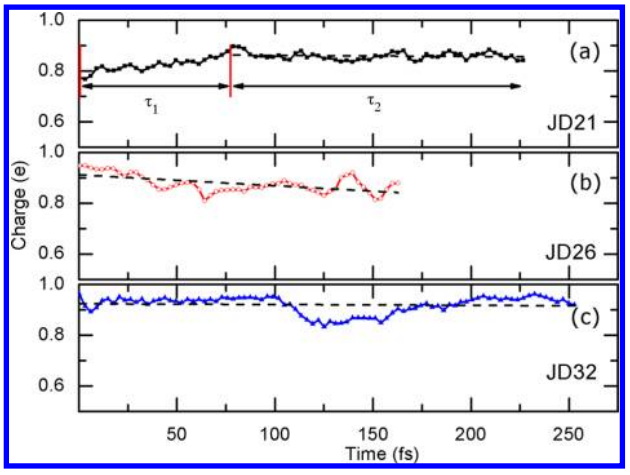

Figure 6. Fraction of average electrons transferred back from the TiO_2 semiconductor substrate to the organic dyes JD21 (a), JD26 (b), and JD32 (c) after excitation at the organic dye−TiO_2 interface. Dashed lines are results fitted by a linear decaying dynamics.

the electron−hole recombination are electronic excited states that correspond to the excitations of an electron from HOMO of the dye to the CB of the TiO_2. We sampled different kinds of initial excitation states, which equal to excitations from HOMO of the dye to different energy states of TiO_2 CB. Note that all these final states are low energy states of TiO_2 CB and do not represent substantial physical differences. The electron−hole recombination process contains two processes: first, the process of thermal fluctuation to thermal equilibrium (τ_1); second, the electron back transfer from TiO_2 conduction band to the dye (τ_2). The thermal equilibrium time is the setup time for electrons relaxing from higher states to the bottom of TiO_2 conduction bands. Ideally, the recombination dynamics displayed in Figure 6 would be linearly decaying as a result of statistical average of many trajectories. However, we have calculated only a few trajectories due to the limit of

dx.doi.org/10.1021/jp410982e | J. Phys. Chem. C 2014, 118, 16447−16457

computational cost. Therefore, some recombination process shows alternatively larger fluctuations around the linearly decaying dynamics (as JD26). As what is shown in Figure 6, immediately after promoting an electron from the HOMO of the dye to the CB of TiO_2, the electrons have a dominant distribution in the CB of the TiO_2. The energy difference between the TiO_2 CBM and the HOMO of the dye drives electrons transfer back from TiO_2 to the sensitizer. The average results of different recombination trajectories show that the occupation of electrons in TiO_2 decay linearly with the time, and apparently dye JD21 (21.25 ps) and JD32 (28.11 ps) have slower recombination rates than dye JD26 (2.12 ps).

3.4. Estimation of DSC Photovoltaic Properties. So far, we have obtained the absorbance of the sensitizer, the photoelectron injection and electron−hole recombination lifetimes in DSC with success. Therefore, the only remaining issue is to put these elements together to calculate the PCE. From eq 1, the PCE of solar cells is determined by the short circuit current and open circuit voltage. So we start with estimating short circuit current, which can be calculated by[1]

$$J_{SC} = \int J(\lambda)\mathrm{d}\lambda = \int \frac{SI}{hc/e\lambda}\mathrm{IPCE}(\lambda)\mathrm{d}\lambda \quad (2)$$

where SI denotes the solar radiation intensity, e is the unit charge, h is the Planck constant, c is the light speed in vacuum, and IPCE is monochromatic incident phonon to current conversion efficiency, which can be produced using the following equation:[2]

$$\mathrm{IPCE}(\lambda) = \mathrm{LHE}(\lambda)\Phi_{inj}\eta_{coll} \quad (3)$$

Here, the light harvesting efficiency can be calculated with[42]

$$\mathrm{LHE}(\lambda) = \int \varepsilon\rho\, \exp(-\varepsilon\rho x)\mathrm{d}x \quad (4)$$

where x represents the integral of film thickness, ρ is the dye loads of the sensitized TiO_2 electrodes, and ε is the molar extinction coefficient. Substituting IPCE (eq 3) and LHE (eq 4) into eq 2 yields

$$J_{SC} = \iint \frac{SI}{hc/e\lambda}\varepsilon\rho e^{-\varepsilon\rho x} \times \Phi_{inj}\eta_{coll}\mathrm{d}\lambda\mathrm{d}x \quad (5)$$

Therefore, J_{SC} is closely dependent on the light harvesting efficiency, the electron injection efficiency, and collection efficiency. The electron injection and collection efficiency can be expressed as[2,8]

$$\Phi_{inj} = 1/\left(1 + \frac{\tau_{inj}}{\tau_{relax}}\right) \quad (6)$$

$$\eta_{coll} = 1/\left(1 + \frac{\tau_{trans}}{\tau_{rec}}\right) \quad (7)$$

with τ_{inj} being the electron injection lifetime from dye to the TiO_2 substrate, τ_{relax} is the relaxation lifetime for excited state of dye in solution, τ_{trans} denotes the electron transport time for electrons in TiO_2 semiconductor conduction band toward the electrode, and τ_{rec} represents the electron−hole recombination time. As the solvent molecules are not included in our system to avoid heavy computational cost, we do not directly calculate the hot electron relaxation lifetime τ_{relax}. Instead, we assume the τ_{relax} of all these dyes are ∼10 ps according to experiment measurements.[39] Therefore, the calculated injection efficiencies for JD-dyes are 97.2% for JD21, 97.7% for JD26, and 96.2% for JD32, based on eq 6. The estimated η_{coll} is 81.0% for JD21 and 84.9% JD32 if we assume τ_{trans} = 5 ps. However, JD26 has η_{coll} only 29.8%, as a result of its fast recombination time rate. We note that, because of complications in experimental setup such as the presence of solvent and electrolyte molecules, random dye adsorption, and possible aggregation, as well as TiO_2 surface defects, the experimental time scales for the above electron processes are usually several orders of magnitude longer. However, we believe the overall trends for dyes under the same ideal condition (for instance in vacuum) are reasonable. In particular, electron recombination to electrolyte ions is an important process governing energy conversion efficiency in real devices; in principle, this process can be treated in the same way by real-time TDDFT as we do for dye molecules. For the sake of simplicity and considering that electrode−electrolyte recombination is largely blocked by dye layers in optimized devices, we ignore this process at the moment and assume electrode−dye interaction is the dominant recombination pathway.[8] Taking the experiment values of dye loads (300 mmol/L) and the TiO_2 film thickness (10 μm), the calculated J_{SC} are 15.81 mA/cm^2 for JD21, 5.66 mA/cm^2 for JD26, and only 4.77 mA/cm^2 for JD32 (resulting from its poor absorbance in the visible light), which nicely reproduce the experimental 15.4 mA/cm^2 for JD21 and 3.7 mA/cm^2 for JD32[7] (see Table 2; the experimental photovoltaic properties of JD26 have not been available). LHE and IPCE can also be calculated (see Figure 2b,c). Dye JD21 shows good light harvesting and high IPCE properties in the visible light region, in accordance with its high J_{SC}, while the LHE and IPCE of JD32 decay rapidly for light wavelengths above 500 nm, resulting in poor DSC performance for this dye. For JD26, although it possesses good LHE benefiting from broad absorption, the poor electron collection efficiency limits the attainable short circuit current.

Table 2. Estimations of Conduction Band Minimum, Redox Potential, n_c, the Calculated and Corresponding Experiment Open Circuit Voltage V_{OC} of JD-Dyes Based on Model-I

dye	E_{CBM} (eV)	E_{redox} (eV)	ΔE_1[a] (eV)	n_c (cm^{-3})	ΔE_2[b] (eV)	V_{OC} (mV)	V_{OC} (exp; mV)
JD21	−3.59	−5.04	1.45	2.42×10^{19}	−0.087	1363	730
JD26	−3.63	−5.04	1.41	2.23×10^{19}	−0.089	1321	
JD32	−3.63	−5.04	1.41	1.69×10^{16}	−0.275	1135	553

[a] $\Delta E_1 = E_{CBM} - E_{redox}$. [b] $\Delta E_1 = k_B T \ln(n_c/N_{CB})$.

The open circuit voltage, V_{OC}, which is defined as the potential difference between the electrolyte redox potential and the quasi-Fermi level of electrons in the semiconductor TiO_2, can be calculated with the empirical formulas below (model-I),[27]

$$V_{OC} = \frac{E_{CBM} - E_{redox} + \Delta CB}{q} + \frac{k_B T}{q}\ln\left(\frac{n_c}{N_{CB}}\right) \quad (8)$$

where N_{CB} is the accessible density of conduction band states in the semiconductor; n_c is the number of injected electrons in TiO_2 due to dye adsorption; and ΔCB is the shift of E_{CBM} when the dyes are adsorbed on TiO_2, related to the surface dipole upon dye adsorption and dye concentration on the substrate. Obviously, the contributions of dye loads and dye adsorption have already been taken into consideration in our slab model

dx.doi.org/10.1021/jp410982e | J. Phys. Chem. C 2014, 118, 16447−16457

Table 3. Estimations of Injection and Recombination Rates and Photovoltaic Device Data Using TDDFT Simulations

dye	k^{-1}_{inj} (fs)	k^{-1}_{rec} (ps)	J_{sc} (mA·cm^2)	V_{OC} (mV)	FF	J_{sc}(exp; mA·cm^2)	V_{OC}(exp; mV)	FF (exp)	η (%)	η (exp; %)
JD21	290	20.25	15.81	732	0.85	15.4	730	0.75	9.84	8.4
JD26	240	2.12	5.66	509	0.81				2.33	
JD32	400	28.11	4.77	676	0.84	3.7	553	0.78	2.71	1.7

calculations of the dye/TiO_2 composite system. In general, different dye load results in a different surface blocking layer, which affects electron recombination rates. The difference in dye binding configurations also leads to different surface dipole moments, which shift the energy level of CBM. In our system, by directly modeling dye/TiO_2 interface, the calculated E_{CBM} has already included the energy shift caused by dye adsorption. The temperature of 300 K and typical N_{CB} density of 7×10^{20} cm^{-3} are adopted according to the experiment.[43] n_c is calculated with the intergral of wave function distributions on the TiO_2 substrate of the LUMO orbital of the chromophore. As a result, the V_{OC} based on model-I are obtained and listed in Table 2.

From Table 2, the calculated V_{OC} of JD21 and JD26 are 1.36, 1.32, and 1.14 V for JD32, almost two times larger than the experiment results (730 mV for JD21 and 553 mV for JD32 under standard global AM1.5G illumination with 10 μm thick TiO_2).[7] If we adjust N_{CB} to match the calculated V_{OC} to experimental values, the N_{CB} would be $\sim 10^{30}$ cm^{-3}, highly unrealistic in real system. Apparently, model-I is too superficial to understand the origin of V_{OC} in DSC, which considers dye loads and surface dipole effects but neglects the recombination contribution. The open-circuit voltage, which is set by the maximum separation between the Fermi level of electrons in TiO_2 and the electrochemical potential of the holes/ions in holes transfer materials, is strongly limited by the electron−hole recombination.

Given that electron and hole transport materials are spatially close to each other in the nanostructured configuration of DSC, electrons in TiO_2 conduction band easily recombine with the holes in sensitizers and solution if not efficiently transport to the electrode contact, resulting in lowering in the Fermi level of electrons in TiO_2 and a decrease in V_{OC}. Therefore, the influence of recombination rates on V_{OC} should be taken into consideration. More realistic method to evaluate V_{OC} involves the charge recombination effects and should give nice predictions of V_{OC}, which reads (model-II):[26]

$$V_{OC} = \frac{k_B T}{\beta' q} \ln \frac{\beta' q R_0 J_{SC}}{k_B T} \tag{9}$$

where β' is the charge transfer coefficient for recombination of electrons (taking the empirical value of 0.45). R_0 is the recombination resistance, which is defined as

$$R_0 = \frac{\sqrt{\pi \lambda k_B T}}{q^2 d \gamma k_{rec} c_{ox} N_s} \exp\left(\gamma \frac{E_{CBM} - E_{redox}}{k_B T} + \frac{\lambda}{4 k_B T}\right) \tag{10}$$

Here d is the film thickness (we adopt the experiment value 10 μm),[7] c_{ox} is concentration of acceptor species (I_3^-, ~50 mmol/L), N_S is a constant related to the total number of surface states contributing to recombination ($\sim 10^5$), γ is related to electron trap distribution below CB (~0.3), k_{rec} is the electron recombination rate, λ corresponds to the reorganization energy that can be obtained from DFT calculations on molecules in solution.[44] E_{redox} is the reduction−oxidation potential of electrolyte (set as standard iodide/triiodide redox potential: −5.04 eV). Therefore, we could calculate the open circuit voltage V_{OC}, which are 732, 509, and 676 mV for JD21, JD26, and JD32 dyes, respectively. JD26 possesses a low V_{OC} because of its faster charge recombination. These results agree well with the experiment values (730 mV for JD21 and 553 mV for JD32, see Table 3).[7] In addition, according to the photocurrent−photovoltage properties of solar cells, the $I-V$ curve of DSC can be depicted in the presence of known V_{OC} and J_{SC}:

$$V = \frac{k_B T}{q} \ln\left(\frac{J_{sc} - I}{I_S} + 1\right) \tag{11}$$

here, I_S is the reverse saturation current,

$$I_S = \frac{J_{SC}}{\exp(q V_{OC}/k_B T) - 1} \tag{12}$$

Figures 2d and 3d show the calculated $I-V$ curve of JD-dyes and L-dyes. With the maximum output power (can be directly calculated from the $I-V$ curve) divided by J_{SC} and V_{OC}, we got the fill factor of the system. Finally, we obtain the PCE of JD-dyes, which are 9.84, 2.33, and 2.71% for JD21, JD26, and JD32, respectively, with errors below 1−2% comparing with the experiment (8.4% for JD21 and 1.7% for JD32). Note that among the above steps to evaluate the PCE of DSC, only one empirical parameter, the recombination coefficient β', is adopted; others, like the energy levels, the reorganization energy λ, and the injection (recombination) rates, can be directly calculated using the tools of first principles simulations. The rest of the parameters are all experimental settings (or properties not related to the dye molecule).

Until now, we have successfully achieved our goal of precisely predicting the solar cells efficiency and related photovoltaic performance by using the tools of first principle simulations. Ground state electronic structures and especially the excited state electronic dynamics are calculated based on DFT and TDDFT, making it possible to predict the PCE of DSC with standard experimental settings and few empirical parameters. The estimated solar cell efficiencies of model systems are consistent with corresponding experimental values, with errors below 1−2%. LHE, IPCE, and $I-V$ curves are also well reproduced and are comparable with experiment. On one hand, the predicted efficiency can serve as the efficiency limit for a given dye performing under ideal conditions, providing guidance for device optimization to achieve its optimal performance. On the other hand, this model essentially serves as a "virtual device", whose characteristics change as the "experimental" settings (dye concentration, film thickness, type of solvents, etc.) change. By manually changing these set-ups, the model forecasts photovoltaic performances of a real device under the same condition.

3.5. Empirical Models for Estimating Electron Injection and Recombination Rate. However, the above procedure for estimating DSC efficiency from first principles electron dynamics is computationally very time-consuming (mainly on the real time simulations of electron injection and charge recombination), limiting the large-scale applications of this theoretical approach. It would be better if the injection and

dx.doi.org/10.1021/jp410982e | J. Phys. Chem. C 2014, 118, 16447−16457

Table 4. Estimation of Driving Forces, Reorganization Energies, Charge Transfer Distances, Injection and Recombination Rates, and Corresponding Photovoltaic Data for JD-Dyes and L-Dyes Based on Marcus Theory

dye	λ^a (eV)	$\Delta G^*_{inj}{}^b$ (eV)	$\Delta G^*_{rec}{}^b$ (eV)	r_{inj} (Å)	r_{rec} (Å)	β (Å^{-1})	k^{-1}_{inj} (fs)	k^{-1}_{rec} (ps)	J_{sc} (mA·cm^2)	V_{OC} (mV)	FF	η (%)
JD21	1.22	0.092	0.055	2.34	9.75	0.7	476	20.30	15.40	728	0.85	9.53
JD26	1.21	0.110	0.033	2.35	6.59	0.7	960	0.95	2.86	423	0.78	0.94
JD32	1.26	0.008	0.003	2.37	13.55	0.7	19	39.62	5.17	701	0.85	3.08
L0	1.46	0.155	0.012	2.27	9.04	0.48	387	8.65	3.37	739	0.85	2.12
L1	1.40	0.197	0.022	2.24	14.84	0.26	351	7.80	5.53	741	0.85	3.48
L2	1.32	0.197	0.026	2.06	16.79	0.23	356	8.89	7.79	715	0.85	4.73

[a]The reorganization energy λ is assumed to be the same for both injection and recombination. [b]$\Delta G^* = (-\Delta G^0 + \lambda)^2/4\lambda$.

recombination lifetimes can be calculated using a simpler way. Luckily, Marcus theory lights us with an effective solution. According to Marcus theory,[45] the nonadiabatic electron transfer rate between two centers held at the fixed distance and orientation is

$$k_{ET} = A\sqrt{\frac{\pi}{\hbar^2 \lambda k_B T}}\ \exp(-\beta r)\ \exp\left(\frac{-(-\Delta G^0 + \lambda)^2}{4\lambda k_B T}\right) \quad (13)$$

In eq 13, ΔG^0 is the driving force for the reaction, r is the electron transfer distance, β is the attenuation factor, and A is a constant.

Previous studies of the wave functions of the JD-dyes HOMO and LUMO orbital reveal that the HOMO is mainly delocalized around periphery of the ullazine heterocycle while the LUMO basically resides on the anchoring cyanoacetic acid group.[7] During the injection process, electron transfers from the LUMO orbital of the dye to the TiO_2 CB. Thus, the transfer distance of the injection process r_{inj} is between the cyanoacrylic acid anchoring group and the TiO_2 surface, while for the recombination process, electrons transfer back from the TiO_2 CB to the HOMO orbital of the dye. The transfer distance r_{rec} is defined by the distance between the donor moiety (the central nitrogen atom) of the dye to the TiO_2 interface. The injection and recombination distance can also be obtained by calculating the average electrostatic potentials in the vertical direction (see Supporting Information, Figures S2 and S3). Finally, the injection and recombination lifetime in DSC can be obtained. The estimation of reorganization energies, activation energies, charge transfer distances, and rates for the injection and recombination dynamics is given in Table 4.

Based on the Marcus theory, the injection and recombination rates of JD-dyes and L-dyes are easily attained, shown in Table 4. We note that with selected parameters the recombination lifetimes of JD-dyes are similar to our simulation results using TDDFT (20.3 ps vs 20.25 ps for JD21, 0.95 ps vs 2.12 ps for JD26, 39.62 ps vs 28.11 ps for JD32). But the injection rates show much discrepancy, with injection rates of JD21 and JD26 two times larger than the TDDFT results, while JD32 exhibits inverse tendency (10× smaller than the simulation value). Although the calculated injection rates based on the semiclassical model do not agree well with the simulation results, the corresponding photovoltages and photocurrents are similar, which are in good agreement with the experiment.

For L-dyes, as the thickness of the mesoporous TiO_2 film is 3 μm in experiment, we assume the τ_{trans} = 2 ps. The η_{coll} are ~85% for the three dyes. The calculated photovoltaic parameters of L-dyes also reproduce nicely the experiment values (see Supporting Information, Table S1).[37] Taking dye L0 as an example, the calculated J_{SC} is 3.37 mA/cm^2 versus 2.89 mA/cm^2 in experiment, and the V_{OC} is 739 mV versus 735 mV in experiment. Figure 3c,d shows the calculated IPCE and $I-V$ curve of L-dyes with the injection and recombination rates calculated by Marcus theory.

Note that the attenuation factors for L-dyes are distinct for each dye, which is actually tuned by a mathematic trick (attenuation factors adjusted to approach the experiment results). As a matter of fact, the real charge transfer dynamics at dye/TiO_2 interface is a complicated issue with changing electronic structures and interfacial configurations. Although the semiclassical Marcus theory has considered the influences of driving force and charge transfer distance on the interface electron transfer, the empirical model can only qualitatively but not quantitatively describe the interface electronic dynamics. Therefore, the TDDFT based real-time evolution of electronic dynamics at dye/TiO_2 interface gives more insightful theoretical understanding of the atomistic energy conversion mechanism with no or few empirical parameters and, thus, are most desirable.

4. CONCLUSION

In conclusion, we present a new systematic approach to accurately estimate the photovoltaic properties of dye sensitized solar cells. Two kinds of D-π-A dyes are adopted as sample dyes. The short circuit current can be precisely predicted by calculating the dyes' photo absorption and the electron injection and recombination lifetime using real-time excited state electronic dynamics simulations based on TDDFT. Open circuit voltage can be nicely reproduced by calculating the voltage difference between the quasi-Fermi level of electrons in the semiconductor substrate and the electrolyte redox potential, with the influence of electron recombination included. Based on the real time TDDFT dynamics simulations, the estimated power conversion efficiency of DSC fits nicely with the experiment, with deviation below 1−2%. Light harvesting efficiency, incident photon-to-electron conversion efficiency (IPCE) and the current−voltage ($I-V$) characteristics can also be well reproduced. This work presents a set of predictive algorithms for nanodevice operation rate assessment (PANDORA). Our method is demonstrated to be an accurate and efficient strategy for dye design and DSC optimization.

■ ASSOCIATED CONTENT

Supporting Information

Projected density of states for L-dyes, electrostatic potential for JD- and L-dyes, and experimental device parameters for L-dyes are provided. This information is available free of charge via the Internet at http://pubs.acs.org

dx.doi.org/10.1021/jp410982e | J. Phys. Chem. C 2014, 118, 16447−16457

AUTHOR INFORMATION

Corresponding Author

*Tel.: + 86-10-82649396. E-mail: smeng@iphy.ac.cn.

Notes

The authors declare no competing financial interest.

ACKNOWLEDGMENTS

We acknowledge financial supports from the NSFC (Grants 11222431 and 11074287), the MOST (2012CB921403), and the hundred-talent program of CAS.

REFERENCES

(1) O'Regan, B.; Gratzel, M. A Low-Cost, High-Efficiency Solar Cell Based on Dye-Sensitized Colloidal TiO_2 Films. *Nature* **1991**, *353*, 737−740.

(2) Yella, A.; Lee, H.-W.; Tsao, H. N.; Yi, C.; Chandiran, A. K.; Nazeeruddin, M. K.; Diau, E. W.-G.; Yeh, C.-Y.; Zakeeruddin, S. M.; Grätzel, M. Porphyrin-Sensitized Solar Cells with Cobalt (II/III)-Based Redox Electrolyte Exceed 12% Efficiency. *Science* **2011**, *334*, 629−634.

(3) Burschka, J.; Pellet, N.; Moon, S.-J.; Humphry-Baker, R.; Gao, P.; Nazeeruddin, M. K.; Gratzel, M. Sequential Deposition as a Route to High-Performance Perovskite-Sensitized Solar Cells. *Nature* **2013**, *499*, 316−319.

(4) Zhang, M.; Wang, Y.; Xu, M.; Ma, W.; Li, R.; Wang, P. Design of High-Efficiency Organic Dyes for Titania Solar Cells Based on the Chromophoric Core of Cyclopentadithiophene-Benzothiadiazole. *Energy Environ. Sci.* **2013**, *6*, 2944−2949.

(5) Chiba, Y.; Islam, A.; Watanabe, Y.; Komiya, R.; Koide, N.; Han, L.; Komiya, R.; Koide, N.; Han, L. Y. Dye-Sensitized Solar Cells with Conversion Efficiency of 11.1%. *Jpn. J. Appl. Phys* . **2006**, *45*, 638−640.

(6) Hardin, B. E.; Sellinger, A.; Moehl, T.; Humphry-Baker, R.; Moser, J.-E.; Wang, P.; Zakeeruddin, S. M.; Grätzel, M.; McGehee, M. D. Energy and Hole Transfer Between Dyes Attached to Titania in Cosensitized Dye-Sensitized Solar Cells. *J. Am. Chem. Soc.* **2011**, *133*, 10662−10667.

(7) Delcamp, J. H.; Yella, A.; Holcombe, T. W.; Nazeeruddin, M. K.; Grätzel, M. The Molecular Engineering of Organic Sensitizers for Solar-Cell Applications. *Angew. Chem., Int. Ed.* **2013**, *52*, 376−380.

(8) Haid, S.; Marszalek, M.; Mishra, A.; Wielopolski, M.; Teuscher, J.; Moser, J.-E.; Humphry-Baker, R.; Zakeeruddin, S. M.; Grätzel, M.; Bäuerle, P. Significant Improvement of Dye-Sensitized Solar Cell Performance by Small Structural Modification in π-Conjugated Donor−Acceptor Dyes. *Adv. Funct. Mater.* **2012**, *22*, 1291−1302.

(9) Labat, F.; Le Bahers, T.; Ciofini, I.; Adamo, C. First-Principles Modeling of Dye-Sensitized Solar Cells: Challenges and Perspectives. *Acc. Chem. Res.* **2012**, *45*, 1268−1277.

(10) Jacquemin, D.; Perpete, E. A.; Scuseria, G. E.; Ciofini, I.; Adamo, C. TD-DFT Performance for the Visible Absorption Spectra of Organic Dyes: Conventional Versus Long-Range Hybrids. *J. Chem. Theory Comput.* **2007**, *4*, 123−135.

(11) Becke, A. D. Density-Functional Thermochemistry. III. The Role of Exact Exchange. *J. Chem. Phys.* **1993**, *98*, 5648−5652.

(12) Beek, W. J. E.; Janssen, R. A. J. Spacer Length Dependence of Photoinduced Electron Transfer in Heterosupramolecular Assemblies of TiO_2 Nanoparticles and Terthiophene. *J. Mater. Chem.* **2004**, *14*, 2795−2800.

(13) Chang, C.-W.; Luo, L.; Chou, C.-K.; Lo, C.-F.; Lin, C.-Y.; Hung, C.-S.; Lee, Y.-P.; Diau, E. W.-G. Femtosecond Transient Absorption of Zinc Porphyrins with Oligo(phenylethylnyl) Linkers in Solution and on TiO_2 Films.[†]. *J. Phys. Chem. C* **2009**, *113*, 11524−11531.

(14) Manzhos, S.; Segawa, H.; Yamashita, K. Derivative Coupling Constants of NK1, NK7 Dyes and Their Relation to Excited State Dynamics in Solar Cell Applications. *Chem. Phys. Lett.* **2011**, *501*, 580−586.

(15) Persson, P.; Lundqvist, M. J.; Ernstorfer, R.; Goddard, W. A.; Willig, F. Quantum Chemical Calculations of the Influence of Anchor-Cum-Spacer Groups on Femtosecond Electron Transfer Times in Dye-Sensitized Semiconductor Nanocrystals. *J. Chem. Theory Comput.* **2006**, *2*, 441−451.

(16) Abuabara, S. G.; Rego, L. G. C.; Batista, V. S. Influence of Thermal Fluctuations on Interfacial Electron Transfer in Functionalized TiO_2 Semiconductors. *J. Am. Chem. Soc.* **2005**, *127*, 18234−18242.

(17) Kilina, S. V.; Kilin, D. S.; Prezhdo, V. V.; Prezhdo, O. V. Theoretical Study of Electron−Phonon Relaxation in PbSe and CdSe Quantum Dots: Evidence for Phonon Memory. *J. Phys. Chem. C* **2011**, *115*, 21641−21651.

(18) Long, R.; Prezhdo, O. V. Ab Initio Nonadiabatic Molecular Dynamics of the Ultrafast Electron Injection from a PbSe Quantum Dot Into the TiO_2 Surface. *J. Am. Chem. Soc.* **2011**, *133*, 19240−19249.

(19) Stier, W.; Duncan, W. R.; Prezhdo, O. V. Thermally Assisted Sub-10 fs Electron Transfer in Dye-Sensitized Nanocrystalline TiO_2 Solar Cells. *Adv. Mater.* **2004**, *16*, 240−244.

(20) Li, J.; Nilsing, M.; Kondov, I.; Wang, H.; Persson, P.; Lunell, S.; Thoss, M. Dynamical Simulation of Photoinduced Electron Transfer Reactions in Dye−Semiconductor Systems with Different Anchor Groups. *J. Phys. Chem. C* **2008**, *112*, 12326−12333.

(21) Jones, D. R.; Troisi, A. A Method to Rapidly Predict the Charge Injection Rate in Dye Sensitized Solar Cells. *Phys. Chem. Chem. Phys.* **2010**, *12*, 4625−4634.

(22) Li, Z.; Zhang, X.; Lu, G. Dipole-Assisted Charge Separation in Organic−Inorganic Hybrid Photovoltaic Heterojunctions: Insight from First-Principles Simulations. *J. Phys. Chem. C* **2012**, *116*, 9845−9851.

(23) Duncan, W. R.; Craig, C. F.; Prezhdo, O. V. Time-Domain ab Initio Study of Charge Relaxation and Recombination in Dye-Sensitized TiO_2. *J. Am. Chem. Soc.* **2007**, *129*, 8528−8543.

(24) Ma, W.; Jiao, Y.; Meng, S. Modeling Charge Recombination in Dye-Sensitized Solar Cells Using First-Principles Electron Dynamics: Effects of Structural Modification. *Phys. Chem. Chem. Phys.* **2013**, *15*, 17187−17194.

(25) Meng, S.; Kaxiras, E. Mechanisms for Ultrafast Nonradiative Relaxation in Electronically Excited Eumelanin Constituents. *Biophys. J.* **2008**, *95*, 4396−4402.

(26) Raga, S. R.; Barea, E. M.; Fabregat-Santiago, F. Analysis of the Origin of Open Circuit Voltage in Dye Solar Cells. *J. Phys. Chem. Lett.* **2012**, *3*, 1629−1634.

(27) Marinado, T.; Nonomura, K.; Nissfolk, J.; Karlsson, M. K.; Hagberg, D. P.; Sun, L.; Mori, S.; Hagfeldt, A. How the Nature of Triphenylamine-Polyene Dyes in Dye-Sensitized Solar Cells Affects the Open-Circuit Voltage and Electron Lifetimes. *Langmuir* **2009**, *26*, 2592−2598.

(28) Kohn, W.; Sham, L. J. Self-Consistent Equations Including Exchange and Correlation Effects. *Phys. Rev.* **1965**, *140*, A1133−A1138.

(29) Soler, J. M.; Artacho, E.; Gale, J. D.; Garcia, A.; Junquera, J.; Ordejon, P.; Sanchez-Portal, D. The SIESTA Method for Ab Initio Order-N Materials Simulation. *J. Phys.: Condens. Matter* **2002**, *14* (11), 2745.

(30) Troullier, N.; Martins, J. L. Efficient Pseudopotentials for Plane-Wave Calculations. *Phys. Rev. B* **1991**, *43*, 1993−2006.

(31) Artacho, E.; Angalada, E.; Dieguez, O.; Gale, J. D.; Junquera, J.; Martin, R. M.; Ordejon, P.; Pruneda, J. M.; Sanchez-Portal, D.; Soler, J. M. The SIESTA Method: Developments and Applicability. *J. Phys.: Condens. Matter* **2008**, *20*, 064208.

(32) Junquera, J.; Zimmer, M.; Ordejón, P.; Ghosez, P. First-Principles Calculation of the Band Offset at $BaO/BaTiO_3$ and $SrO/SrTiO_3$ Interfaces. *Phys. Rev. B* **2003**, *67*, 155327.

(33) Lazzeri, M.; Vittadini, A.; Selloni, A. Erratum: Structure and Energetics of Stoichiometric TiO_2 Anatase Surfaces. *Phys. Rev. B* **2002**, *65*, 119901.

(34) Cossi, M.; Rega, N.; Scalmani, G.; Barone, V. Energies, Structures, and Electronic Properties of Molecules in Solution with the C-PCM Solvation Model. *J. Comput. Chem.* **2003**, *24*, 669−681.

(35) Meng, S.; Kaxiras, E. Real-Time, Local Basis-Set Implementation of Time-Dependent Density Functional Theory for Excited State Dynamics Simulations. *J. Chem. Phys.* **2008**, *129*, 054110−054112.
(36) Jiao, Y.; Zhang, F.; Grätzel, M.; Meng, S. Structure−Property Relations in All-Organic Dye-Sensitized Solar Cells. *Adv. Funct. Mater.* **2013**, *23*, 424−429.
(37) Hagberg, D. P.; Marinado, T.; Karlsson, K. M.; Nonomura, K.; Qin, P.; Boschloo, G.; Brinck, T.; Hagfeldt, A.; Sun, L. Tuning the HOMO and LUMO Energy Levels of Organic Chromophores for Dye Sensitized Solar Cells. *J. Org. Chem.* **2007**, *72*, 9550−9556.
(38) Meng, S.; Ren, J.; Kaxiras, E. Natural Dyes Adsorbed on TiO_2 Nanowire for Photovoltaic Applications: Enhanced Light Absorption and Ultrafast Electron Injection. *Nano Lett.* **2008**, *8*, 3266−3272.
(39) Cherepy, N. J.; Smestad, G. P.; Grätzel, M.; Zhang, J. Z. Ultrafast Electron Injection: Implications for a Photoelectrochemical Cell Utilizing an Anthocyanin Dye-Sensitized TiO_2 Nanocrystalline Electrode. *J. Phys. Chem. B* **1997**, *101*, 9342−9351.
(40) Huber, R.; Moser, J.-E.; Grätzel, M.; Wachtveitl, J. Real-Time Observation of Photoinduced Adiabatic Electron Transfer in Strongly Coupled Dye/Semiconductor Colloidal Systems with a 6 fs Time Constant. *J. Phys. Chem. B* **2002**, *106*, 6494−6499.
(41) Meng, S.; Kaxiras, E. Electron and Hole Dynamics in Dye-Sensitized Solar Cells: Influencing Factors and Systematic Trends. *Nano Lett.* **2010**, *10*, 1238−1247.
(42) Vlachopoulos, N.; Liska, P.; Augustynski, J.; Graetzel, M. Very Efficient Visible Light Energy Harvesting and Conversion by Spectral Sensitization of High Surface Area Polycrystalline Titanium Dioxide Films. *J. Am. Chem. Soc.* **1988**, *110*, 1216−1220.
(43) Marinado, T.; Hagberg, D. P.; Hedlund, M.; Edvinsson, T.; Johansson, E. M. J.; Boschloo, G.; Rensmo, H.; Brinck, T.; Sun, L.; Hagfeldt, A. Rhodanine Dyes for Dye-Sensitized Solar Cells: Spectroscopy, Energy Levels and Photovoltaic Performance. *Phys. Chem. Chem. Phys.* **2009**, *11*, 133−141.
(44) Zhang, J.; Li, H.-B.; Sun, S.-L.; Geng, Y.; Wu, Y.; Su, Z.-M. Density Functional Theory Characterization and Design of High Performance Diarylamine-Fluorene Dyes with Different π Spacers for Dye-Sensitized Solar Cells. *J. Mater. Chem.* **2012**, *22*, 568−576.
(45) Meade, T. J.; Gray, H. B.; Winkler, J. R. Driving-Force Effects on the Rate of Long-Range Electron Transfer in Ruthenium-Modified Cytochrome C. *J. Am. Chem. Soc.* **1989**, *111*, 4353−4356.